J. Fluid Mech. (1994), *vol.* 263, *pp.* 63–92

Periodically arranged co-flowing jets

By E. VILLERMAUX AND E. J. HOPFINGER
Institut de Mécanique de Grenoble/LEGI-CNRS, BP 53X, 38041 Grenoble Cedex, France

(Received 15 December 1992 and in revised form 20 September 1993)

The problem of a periodic planar arrangement of a large number of co-flowing, interacting jets is investigated. It is shown that this interaction gives rise to strong near-field oscillations of large-scale spatial coherence and to far-field inhomogeneities. In the experiments performed, the jets were produced behind a flat plate perforated by holes arranged in a square or triangular periodic pattern and placed perpendicular to a uniform flow. At moderate Reynolds numbers, the interaction results in a remarkable low-frequency oscillation of the merging distance of the jets downstream of the plate. A detailed description of the recirculating flow in the cavities between the jets emphasizes the role of the backflow in the cavities on the oscillatory behaviour. This description is supported by measurements of the local fluctuating velocity and pressure, two-point correlation measurements and quantitative flow visualizations. These experimental observations suggest a new formulation for the instability dynamics of such unstable recirculating flows. This formulation, based on the nonlinear delayed saturation of the jet's shear layer instability (NLDS model) predicts successfully the dependence of the oscillation of the merging distance on the jet Reynolds number and on the local geometrical features of the confinement of the jets. Furthermore, it is shown that the diffusion of mass coming from one jet, seeded with an inert dye, gives rise to an exponential diffusion front over a distance corresponding to a few mesh sizes indicating a strong local coupling of the jets. At the scale of the whole jet assembly, the oscillations are organized as large-scale travelling waves, propagating from the boundaries of the domain to its centre. This symmetry-breaking property is discussed and supplemented by a spatio-temporal simulation of an array of coupled oscillators.

1. Introduction

Jets are classical turbulent shear flows and numerous studies have been devoted to different aspects of them, motivated either by their widespread engineering applications or by their fundamental interest as a prototype shear flow. Jets are characterized by two modes of instability and consequently by complex structures and are particularly well suited for the study of large-scale and microscale turbulent mixing. A confinement, either by solid walls or by surrounding jets as is considered here can give rise to new flow phenomena. This configuration is of interest in the context of multi-jet burners or liquid propellant rocket engines in that the collective interaction of hindering jets may be coupled with the downstream combustion.

An easy way to produce multiple co-flowing jets is the passage of an air stream through a plate perforated by holes arranged according to a predetermined pattern. This pattern may, for instance, be a two-dimensional periodic network. By varying the hole diameter d with respect to the mesh size M of the network, it is possible to produce multiple jets, when the solid fraction S is high, or interacting wakes. Conceptually, it

is then possible to pass continuously from nearly isolated jets when $M/d \gg 1$ to grid turbulence when $M/d \approx 1$.

Grid turbulence behind low-solidity square-mesh grids has been widely studied (see for instance Comte-Bellot & Corrsin 1966; Groth & Johansson 1988), emphasizing, however, only the far-field ($x > 10M$) homogeneous turbulence. Few results have been reported on high-solidity grid flow which is known to give rise to inhomogeneities of the downstream flow due to jet interaction when the open-area ratio is less than a certain value, about 0.6. Corrsin (1944) reports on experiments made with an array of parallel slots and finds that the flow results from successive coalescence of individual jets. The location of the final large-scale jet is determined by minor inhomogeneities of the grid and/or the upstream flow. Baines & Peterson (1951) show how a uniform upstream velocity profile is distorted in the far field after passage through a grid made of a triangular network of jets with solidity ratio $S = 0.75$. The resulting flow pattern is evolving very slowly in time and the inhomogeneities occur over a scale large compared with the spacing between the jets.

Since the description of the immediate near field of the flow, that is before and up to the jet merging position, was not addressed in these pioneering works, the temporal dynamics of the jet assembly has been ignored. An understanding of this temporal dynamics is of importance in explaining the origin of the flow inhomogeneities downstream of high-solidity grids, or interacting multiple jets like in combustion chambers. Villermaux *et al.* (1991) reported for the first time the existence of a strong self-sustained oscillation of the merging distance of the jets issuing from a square and triangular network of holes. This robust oscillation, which occurs for intermediate jet Reynolds numbers, is locally coherent at the scale of the mesh and develops large-scale propagative instabilities along the network. The flow in the immediate vicinity of the plate was shown to consist of a periodic collection of oscillating jets interacting via adjacent cavities, anchored between the jets, with the spatial periodicity of the network.

This cellular-type oscillating flow pattern is reminiscent of a series of two-dimensional flow configurations which exhibit a very rich variety of large-scale instabilities and auto-organization processes, such as the Rayleigh–Bénard instability above threshold (see Bergé & Dubois 1988; Manneville 1991 for a review), the Faraday instability (Douady 1990) or the dynamics of anchored MHD-driven vortices (Tabeling, Cardoso & Perrin 1990; Somméria 1986). These studies, which were intended to investigate the different routes to turbulence via spatio-temporal intermittency and pattern formation, are now rather well documented experimentally and rely on the systematic theoretical background of complex amplitude equations (see Fauve 1991 for an extensive didactic presentation and van Saarloos & Hohenberg 1992). Although our theoretical approach is somewhat different from the one adopted in these studies, a collection of jets can be considered as a new example of a dynamical system of coupled oscillators.

The paper is organized as follows. After a description of the experimental details and conditions in §2, we present in §3 the results concerning the oscillatory behaviour of the jets and the large-scale properties of the assembly. Then, in §4, a model for these self-sustained oscillations which considers the jets as coupled oscillators is derived from the features of the local flow around the jets. The model predictions concerning the frequency, the spatial coherence of the phase of the oscillations and the mass diffusion along the network are compared with the experimental observations and illustrated by one-dimensional analytical and numerical models.

Finally, the practical implications of our findings are discussed and the qualitative properties of less ordered or networks with defects are commented on.

2. Experimental installation and techniques

The interacting multiple jets were produced by perforated plates, placed in a uniform air stream. Most of the experiments were carried out in a 80×80 cm^2 test-section wind tunnel with a contraction ratio of 16. This wind tunnel, originally designed for the study of the laminar boundary-layer transition has a very low level of residual turbulence. The plates were made of 5 mm thick epoxy. The perforation patterns investigated in this tunnel were square networks of round holes with diameters d equal to 3, 5 and 10 mm and of mesh sizes M equal to 7.6, 12.7, and 25.4 mm respectively, thus giving a constant mesh size to diameter ratio of 2.54 and an expansion ratio for each jet of $4M^2/\pi d^2 = 8.2$. Preliminary experiments were performed in a smaller test-section wind tunnel 15×60 cm^2 in cross-section with contraction ratio 4 and residual turbulence of 0.06%. In this tunnel, the grid was made of a 2 mm thick epoxy plate. For this set of experiments, two perforation patterns were used which are shown on figure 1: a square network of holes $d = 1$ mm in diameter, with $M = 2.54$ mm (this grid is homothetic to the set of grids used in the larger wind tunnel whose solidity ratio is 0.87), and a triangular network of holes $d = 0.8$ mm in diameter and mesh $M = 2.73$ mm, giving a solidity $S = 0.92$.

In all cases, the perforated plates covered the whole section of the wind tunnel and were in contact with the wall to prevent any vibrations on perturbations near the boundaries. The fluctuating velocity measurements were made using one or two independent DISA hot-wire probes which could be accurately positioned in the test section. The measurements of mean velocities were made with a Pitot tube, and for the absolute and fluctuating pressure measurements, a HMB-KWS 3073 differential pressure sensor was used. The frequency response of this pressure transducer depends on the length and diameter of the pressure tube. The tube, placed perpendicular to the flow direction, is 4 mm in diameter and 10 cm long, giving a frequency response of the system of about 450 Hz. The signals were either analysed on-line by a Schlumberger correlator and spectral analyser, or digitized and post-processed on a MASSCOMP 5500 computer.

The lateral walls of the larger wind tunnel are transparent, thus allowing the visualization of the jets. A dense wet, white smoke produced by a high-flow-rate smoke generator was injected through a thin elongated tube located at roughly ten mesh sizes upstream of the plate. The injection velocity of the smoke was set equal to the air velocity in order to minimize the perturbation of the upstream flow. With this facility, it was possible to seed with smoke either an array of jets or a single jet. Then, a plane laser sheet (approximately 1 mm thick) produced by an oscillating mirror (oscillating at about 200 Hz), placed 4 m downstream in the test section, allowed the seeded array to be visualized. The flow, made visual in this way, was recorded using a 25 frames per second CCD video camera positioned at a right angle to the direction of the flow and the laser light plane. The pictures were further analysed on an image processing system.

3. Qualitative observations

3.1. *Mean flow structure of the near field*

In the region immediately behind the grid, the flow reflects the perforation pattern exactly. From each hole an axisymmetric jet issues, which expands with distance from the grid to merge with its neighbours when its diameter has reached a dimension equal to the network mesh size M. We call this merging length $x = L$; it is in the mean

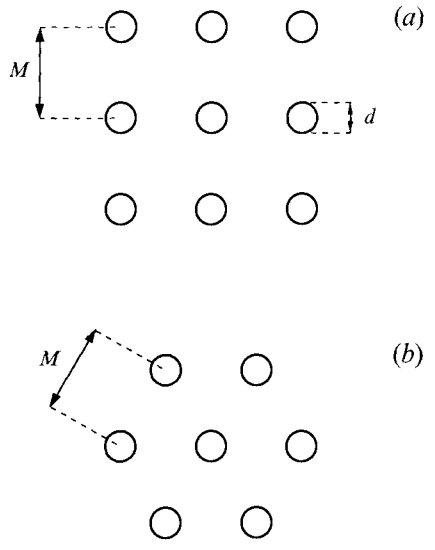

FIGURE 1. Hole patterns: M is the mesh size and d the diameter of the holes. (*a*) Front view, square network. We used a set of grids for which $M/d = 2.54$, with four different diameters: $d = 1$, 3, 5 and 10 mm. (*b*) Front view, triangular network: $M = 2.73$ mm, $d = 0.8$ mm.

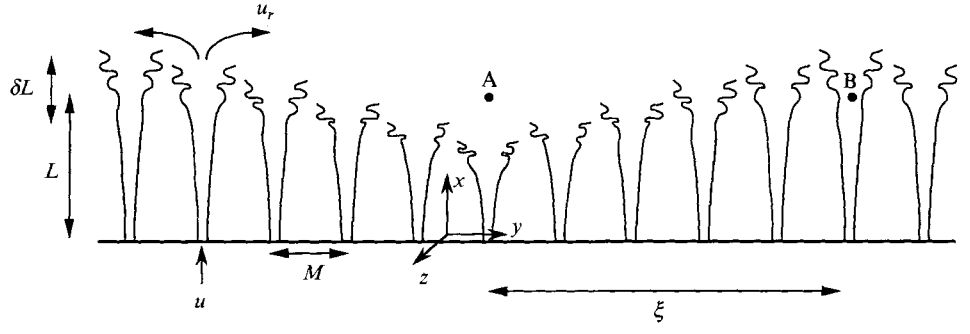

FIGURE 2. Definition sketch of the instantaneous spatial arrangement of an array of jets in a newtork. L is the distance at which the jets merge downstream of the grid, δL is the amplitude of oscillation. The distance ξ between points A and B refers to the correlation length of the pressure along the network. u_r is the typical velocity of the fluid packets shed by a jet at the merging distance, in a direction $r = (y^2+z^2)^{\frac{1}{2}}$ contained in the plane (y, z) parallel to the plate.

homogeneous in the grid plane (y, z) and depends only, for a given geometry of the network, on the jet Reynolds number $Re = ud/\nu$, where u is the velocity (top-hat profiled) at the exit of the jets. Between the jets, before they merge, exists a recirculation flow similar to the recirculating bubble of confined jets or reattaching separated flows behind backward-facing steps for instance. The jet arrangement is shown schematically in figure 2.

When a hot-wire probe located at $x \ll L$ is moved parallel to the grid, it crosses low- and high-velocity regions alternately, with the periodicity of the hole pattern. At the merging position, the fluctuating part of the velocity abruptly increases. Just downstream of the merging position, the time-averaged velocity, which is decreased with respect to the velocity at the centreline of the jets, is nearly uniform and L refers to the position where this uniformity in mean velocity is first observed. So defined, the

uncertainty in the determination of L is within 10% and is consistent with the scaling $uL/\nu = 2 \times 10^4$ with $u(L) \approx \frac{1}{2}u$ (figure 4).

The spreading angle of a laminar jet is known to decrease with increasing Reynolds number, so that, when the jet issues into a confined region of given dimensions, the cavity length is proportional to Re. Above a certain critical Reynolds number, Re_c, instabilities develop progressively, and the mean spreading angle increases with Re to reach the asymptotic value ($\approx 20°$) of turbulent jets. This trend has been observed for a confined jet by Back & Roschke (1972) in the Reynolds-number range 20 to 5×10^3. In Becker & Massaro (1968), this asymptotic regime is reached at Re about 3×10^3 with a single free round jet. The thickness δ of the mixing layer at the nozzle exit in their experiments is $\delta/d = 0.9Re^{-\frac{1}{2}}$ and what they call the 'wave breaking length' L' is found to be $L'/d = 107Re^{-\frac{1}{2}}$. This length L' is in some sense related to our merging length L since it corresponds to the distance from the nozzle exit to the point where the unstable waves suddenly roll up, thus increasing the jet diameter significantly. The above-quoted laws amount to assuming that the characteristic length ξ present in the expression giving the thickness $\delta \sim (\nu\xi/u)^{\frac{1}{2}}$, and which is in fact the length of the boundary-layer development in the nozzle, is equal to the diameter of the nozzle d. Thus, the wavelength λ selected by the Kelvin–Helmholtz instability of the shear layer of thickness δ and which is such that δ/λ is of order unity (Chandrasekhar 1961) is then given by $\lambda/d \sim Re^{-\frac{1}{2}}$, a law which, considering the aspect ratio of the nozzle they used, is actually observed by Becker & Massaro.

If the characteristic lengthscale ξ is the wavelength λ of the preferred unstable mode itself, as is the case if the velocity profile is flat enough at the nozzle exit as in the present experiments, these laws are modified in the following way. In that case, the shear layer starts developing just at the exit of the nozzle, by vorticity diffusion into the surrounding still environment. The instability can thus begin only at a distance x downstream of the nozzle larger than or equal to the wavelength λ predicted by $\delta/\lambda \sim 1$. This condition is satisfied at the critical distance x_c such that $\lambda = x_c \sim (\nu x_c/u)^{\frac{1}{2}}$, giving in this case $\lambda \sim \nu/u$. Therefore, the critical wavenumber of the instability is such that $k_c \sim u/\nu$, and the initial spatial growth rate is proportional to $k_c x$. This relation demonstrates the role of viscosity in the formation of the initial shear layer and in the associated most amplified mode selection and growth rate, explaining the 'earliness' of the onset of the shear instability as a function of Re. The foregoing reasoning remains valid as long as the Reynolds number based on the vorticity thickness of the velocity profile is less than about 100 (Corcos 1979). The effective diameter of the jet at a location x downstream of the nozzle exit is then proportional to ux/ν and is equal to the mesh size M at a distance L from the nozzle exit such that

$$L/M \sim Re^{-1}. \tag{1}$$

This dependence is well supported by our experiments as is seen in figure 3 where the cavity length L, non-dimensionalized by M, is plotted as a function of Re. Also included in this figure is the amplitude of variation of L, denoted by δL, as a function of Re, which will be discussed in §3.2. Note that if the total entrainment flow rate q in the cavity is assumed to be proportional to L and to u in a first approximation, q is constant in the intermediate Reynolds-number range where (1) holds and proportional to u at larger Re. The results of Back & Roschke, replotted in log-log coordinates, exhibit a similar law for reattachment lengths of a jet confined by rigid walls in the transition zone between viscous and turbulent regimes.

We mentioned the existence of a recirculation region, anchored between the jets. The motion inside this region maintains a permanent backflow from the merging position

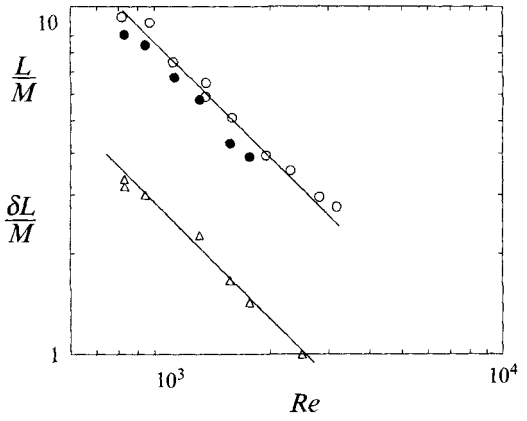

FIGURE 3. Mean merging distance L/M (●, $d = 1$ mm; ○, $d = 5$ mm) and amplitude of oscillation $\delta L/M$ (△, $d = 5$ mm) as a function of the jet Reynolds number Re; square network, $M/d = 2.54$.

towards the jet nozzles. As this backflow will be shown to play a crucial role in the oscillating property of the merging length that we will further describe, it is at this stage worthwhile to discuss its origin and its mean features.

The cavity is, for intermediate Reynolds numbers, laminar, and its aspect ratio M/L is smaller than unity (see figures 3 and 5). The main features of the steady flow may thus be well described in the framework of a lubrication approximation. For simplicity, let us consider a two-dimensional cavity inserted between two jets located at $y = \pm\frac{1}{2}M$. Let $G = (\partial P/\partial x)/\rho$ be the pressure gradient responsible for maintaining the recirculation motion, and let $V(y)$ be the velocity of the fluid in the x-direction parallel to the jet axis. Assuming a quasi-parallel incompressible flow ($\partial^2 V/\partial x^2 \sim u/L^2$; $\partial^2 V/\partial y^2 \sim u/(\frac{1}{2}M)^2$ and $(M/2L)^2 \ll 1$ see figure 3), the lubrication approximation is

$$\frac{1}{\rho}\frac{\partial}{\partial x}P = \nu\frac{\partial^2}{\partial y^2}V(y). \tag{2}$$

The boundary conditions for the velocity are such that $V(\pm\frac{1}{2}M) = u$, with u being the velocity of the jets. The velocity profile is then

$$V(y) = u - \frac{G}{2\nu}[(\tfrac{1}{2}M)^2 - y^2], \tag{3}$$

which is the well-known parabolic shape characteristic of Poiseuille flows.

Up to this point, the pressure gradient G is still unknown but, since we want to describe the steady flow, we have to include in our analysis the fact that the cavity is 'closed' on the average to any mass transport ($q \ll$ recirculation mass flow in the cavity). This implies that the net mass flux, integrated over the total width of the cavity M must be zero, that is

$$\int_{-\frac{1}{2}M}^{+\frac{1}{2}M} V(y)\,\mathrm{d}y = 0. \tag{4}$$

The closure equation (4) determines the pressure gradient as

$$G = 12\nu u/M^2. \tag{5}$$

This pressure gradient is, in usual laboratory conditions, very weak. For instance, at a Reynolds number of 10^3, with $d = 3$ mm and $M = 7.6$ mm, one finds $G = 15$ Pa m^{-1}.

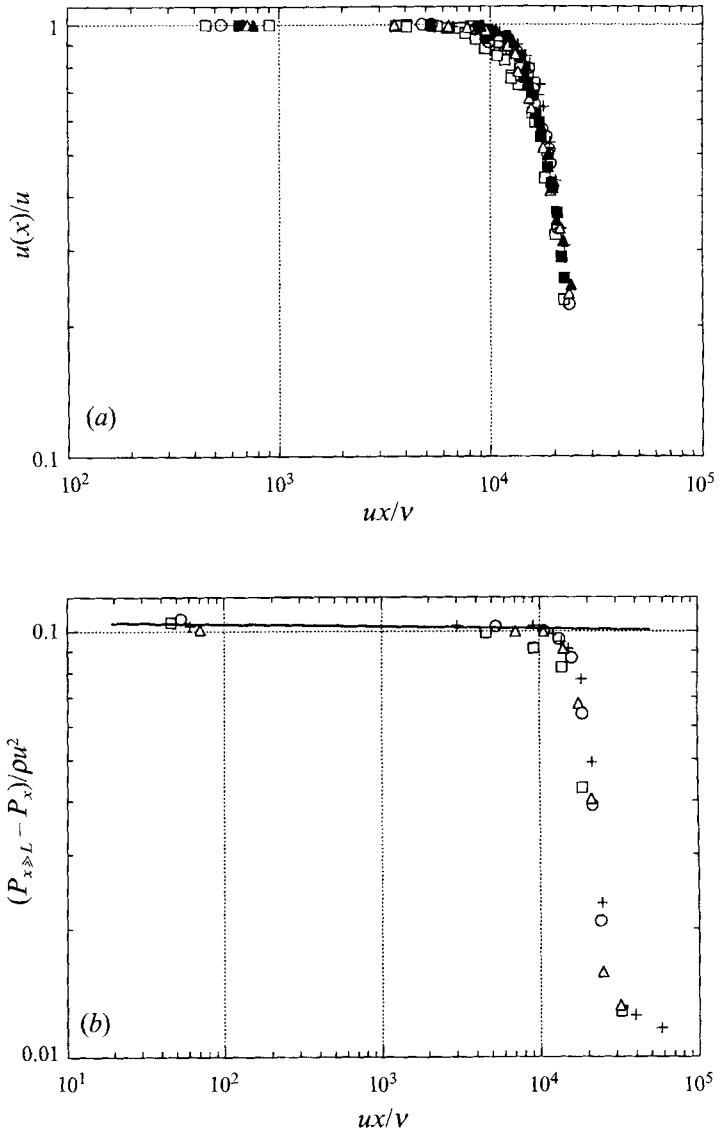

FIGURE 4. (*a*) Decay of the mean velocity $u(x)$ on the centreline of a jet in a square network ($M/d = 2.54$, $d = 3$ mm) a sa function of the rescaled downstream distance ux/ν where u is the nozzle velocity of the jet. The merging distance L is defined such that $uL/\nu \approx 2 \times 10^4$, with $u(L)/u \approx 1/2$. □, $Re = 1350$; ○, $Re = 1600$; +, $Re = 1841$; ■, $Re = 1959$; △, $Re = 2116$; ▲, $Re = 2277$. (*b*) Pressure increase $(P_{x\gg L}-P_x)/\rho u^2$ in a cavity as a function of the rescaled downstream distance ux/ν. $P_{x\gg L}$ is the pressure in the far field downstream of the merging distance and is a constant approximately equal to the ambient pressure.

G is many orders of magnitude less than the gradient G' constructed from the total pressure increase between the plate and the merging length, divided by L. The total pressure increase ΔP is similar to the one obtained through a sudden expansion and is given by

$$\frac{\Delta P}{\rho u^2} = \frac{S_1}{S_2} - \left(\frac{S_1}{S_2}\right)^2, \tag{6}$$

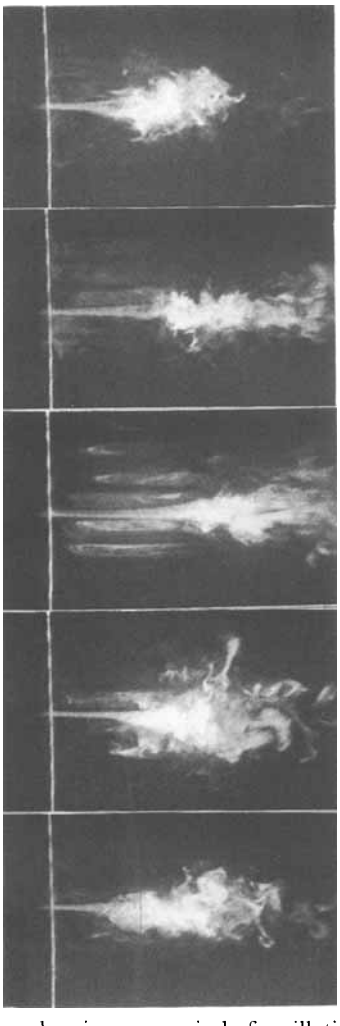

FIGURE 5. Smoke visualizations showing one period of oscillation of a jet ($T = 1$ s) and the interaction with its neighbours. Only one jet imbedded in a square network is seeded with an inert white smoke. The jet is visualized by a laser sheet in the (x, y)-plane; $d = 5$ mm, $M/d = 2.54$, $Re = 943$.

where $S_1 = \frac{1}{4}\pi d^2$ and $S_2 = M^2$. The pressure difference ΔP depends only on the incident kinetic pressure and on the geometry. Thus, writing $G' = \Delta P/\rho L$, and using (1) it is found that the ratio G'/G is of the order

$$\frac{G'}{G} \sim \frac{M}{d} Re^2. \tag{7}$$

Seen at the scale of G', the pressure is nearly constant in the cavity and its gradient hardly detectable (figure 4*b*). Nevertheless, it is sufficient to maintain the motion in the cavity.

As is shown in figure 4(*b*), the evolution of the pressure along the cavity follows the evolution of the velocity measured at the axis of a jet (figure 4*a*). Practically all the available pressure increase occurs at $uL/\nu \approx 2 \times 10^4$, that is to say at the merging distance L, where, by the definition of L, the velocity decreases abruptly. Both the

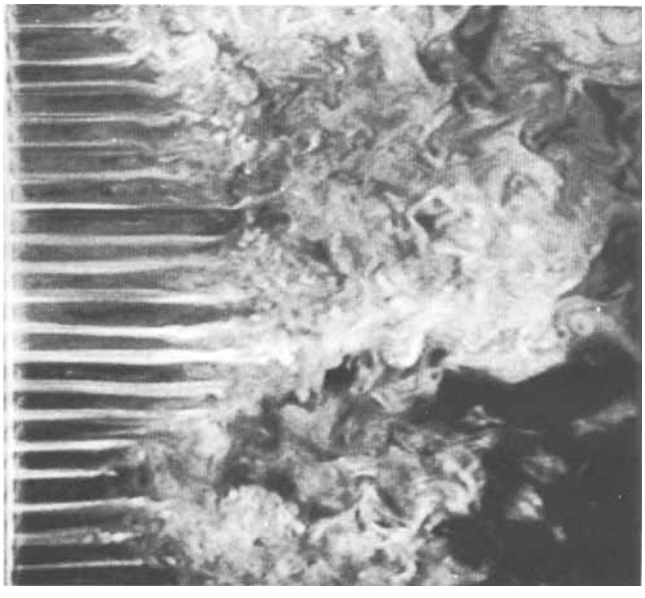

FIGURE 6. Visualization of an array of jets imbedded in a square network seeded with smoke. The instantaneous merging distance varies along the network. Square network, $d = 5$ mm, $M/d = 2.54$, $Re = 730$.

pressure and the velocity are practically constant for $x < L$; only a weak, but measurable positive pressure gradient exists which drives the backflow in the cavities. This observation justifies the lubrication approximation, since it is a proof that, at these Reynolds numbers, the cavity is indeed laminar over the major part of its total length and that the instabilities of the jets are only weakly developed along the cavity up to $x = L$, where the jets finally explode drastically. Flow visualizations demonstrate clearly the sudden destabilization (figure 5).

3.2. *Oscillations*

Beyond a threshold Reynolds number particular to each hole configuration, and up to a Reynolds number of the order of 3×10^3 to 4×10^3, the jets exhibit a remarkable oscillatory property, which still influences the flow far downstream (Villermaux *et al.* 1991 who, however, used a slightly different definition for L). Figure 5 shows a period of oscillation of a jet embedded in the network, seeded with smoke ($Re = 943$). One clearly sees how the merging distance oscillates in time. The existence of a recirculating flow in the adjacent cavities is also demonstrated as well as the spatial extent of the coupling between the jets. At the merging distance with its first neighbours, the jet 'explodes' and throws turbulent fluid packets around itself, up to its fourth or fifth neighbour. These packets are then convected upstream by the backflow in the cavities. When a complete array of jets is seeded, the resulting spatial coherence is even more clearly seen (figure 6).

The phenomenon is also obvious from velocity records obtained with a probe located at the edge of a jet, close to the merging region. One sees from figure 7 that the signals display spikes (strong decreases of velocity) that are fairly periodic. These relate the residence times of the probe in the turbulent region downstream of the merging, where the mean velocity is much less than in the core of the jet (about ten times smaller depending on the value of the solidity ratio). At the same time, a

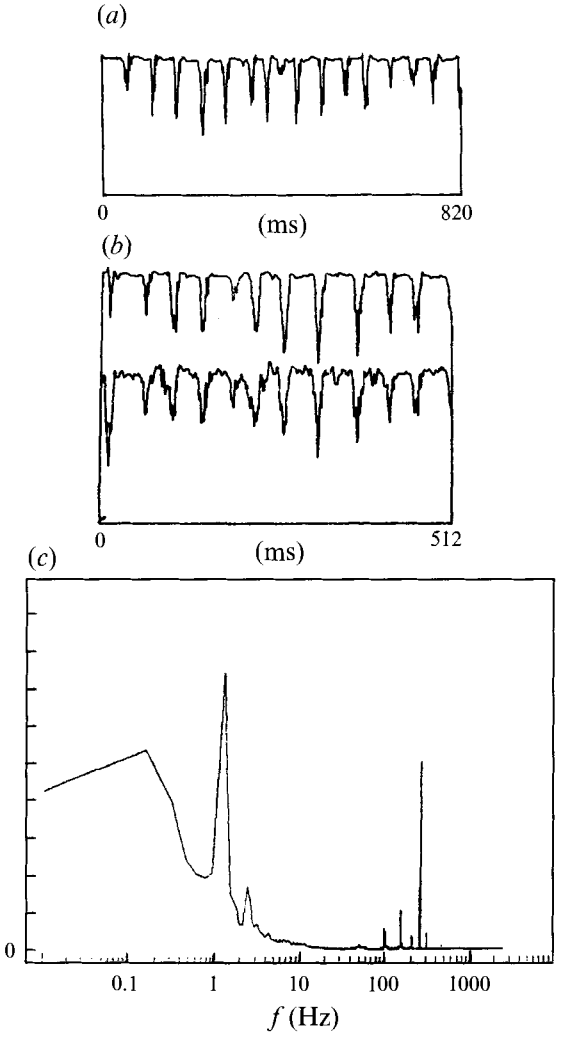

FIGURE 7. Velocity signal recorded by a probe positioned at $x = L$ in the centreline of a jet (square network, $d = 1$ mm, $Re = 1923$). (*b*) Simultaneous signals recorded by two probes positioned on opposite sides of a jet showing that the motion of the merging distance is axisymmetric (square grid, $d = 1$ mm, $Re = 1923$). (*c*) Spectrum of the velocity fluctuations recorded with a probe positioned at the edge of a jet. The low-frequency peak corresponds to the oscillation of the merging distance of the jet, and the high-frequency peak relates to the shedding of the Kelvin–Helmholtz roll-up vortices associated with a Strouhal number $fd/u \approx 0.4$. (Square network, $d = 5$ mm, $Re = 850$).

record at the immediate exit of the hole nozzle inside the jet core reveals a perfect constancy of the velocity indicating that these fluctuations do not affect the incoming flow upstream of the plate (contrary to the observations of Yu, Trouvé & Daily (1991) made in a model ramjet combustor). The fact that the nozzle velocity is not influenced by the downstream oscillations means that the same jet oscillation behaviour would be observed if the jets were to come from individual, non-interconnecting nozzles. If the sensitive part of the probe is exactly positioned on the jet edge (at $x/L \approx 3/4$) the signal also displays the shedding of the Kelvin–Helmholtz roll-up vortices, passing at the usual Strouhal frequency. The resulting spectrum (figure 7*c*), displays both the low-frequency oscillation of the merging distance and the characteristic Strouhal frequency

of the preferred shear mode. These two oscillating modes are decoupled and differ in frequency by about two orders of magnitude.

To check the symmetry of the motion of the jet, it is also possible to use two probes, positioned at opposite sides of a jet (figure 7*b*). The two simultaneous signals are very well correlated, confirming that the oscillation is an axisymmetric motion of the merging length, and not a global flapping of the jet, in accordance with the visualizations (see figure 5 for instance).

The amplitude δL of the motion was measured by positioning a probe at the centreline of a jet, and moving it in the x-direction. The position at which the oscillating motion is first recorded is defined to be $L-\delta L$, since L refers to the position beyond which the uniformity in mean velocity parallel to the grid is reached. This estimation, which compares well with the visualizations, defines δL within the precision of L (roughly 10%). At a fixed Reynolds number, the value of δL is, as L, fairly homogeneous over the entire network. It is shown on figure 3 that $\delta L/M$ obeys an evolution parallel to L/M as a function of Re. For large Reynolds numbers, the amplitude becomes of the order of the mesh size and becomes indistinguishable from the velocity fluctuations in the jet which is, for $Re \approx 3\times 10^3$ and above, already turbulent at the exit of the nozzle. The oscillations thus vanish at high Re and the network consists of 'rigid' stable and non-oscillating jets. The frequency versus jet Reynolds number of all the grid patterns investigated is shown in figure 8(*a*). When rescaled by the mesh size M and velocity u, the frequencies give a Strouhal number $fM/u = 0.007$ (figure 8*b*). This non-dimensional form will be commented on later.

The velocity fluctuations of the recirculating fluid inside a cavity, due to the oscillation of the merging length, and the related pressure fluctuations can be accounted for by hydrodynamic description of the cavity. We already know its steady-state solution at low Reynolds number, given by equations (3) and (5) derived in the previous section. It is worthwhile investigating the complete temporal problem since it will shed light on the experimental simultaneous recordings of the fluctuating pressure and velocity which exhibit a non-trivial phase shift (figure 9).

We rewrite the equation of motion (2), including now the time dependences. Our goal is to relate the fluctuations of velocity in the cavity to an imposed fluctuating pressure gradient $\delta G = a\,\mathrm{e}^{-\mathrm{i}\omega t}$, superimposed on the mean gradient G:

$$\frac{\partial v}{\partial t} = -G + a\,\mathrm{e}^{-\mathrm{i}\omega t} + \nu\frac{\partial^2 v}{\partial y^2}, \tag{8}$$

where $v = v(y,t)$ is the velocity, depending on the space coordinate y and on time t. We have assumed, as previously, a quasi-parallel and incompressible flow. We seek a solution for $v(y,t)$ in the form $v(y,t) = V(y) + \delta v(y,t)$ with

$$\delta v(y,t) = [A\,\mathrm{e}^{\mathrm{i}ky} + B\,\mathrm{e}^{-\mathrm{i}ky} + C]\,\mathrm{e}^{-\mathrm{i}\omega t}, \tag{9}$$

where $V(y)$ is the steady-state solution given by (3); A, B, C and k are, respectively, constants and a wavenumber to be determined. The boundary conditions for $\delta v(y,t)$ are $\delta v(\pm\frac{1}{2}M, t) = 0$. Although lengthy, the computations leading to the solution for $\delta v(y,t)$ are straightforward (see for instance Landau & Lifchitz 1989):

$$\delta v(y,t) = \frac{\mathrm{i}a}{\omega}\mathrm{e}^{-\mathrm{i}\omega t}\left[1 - \frac{\cos(ky)}{\cos(\frac{1}{2}kM)}\right], \tag{10}$$

with

$$k = (1+\mathrm{i})/\zeta \quad \text{and} \quad \zeta = (2\nu/\omega)^{\frac{1}{2}}. \tag{11}$$

The lengthscale ζ is the penetration depth of vorticity in the cavity (skin thickness).

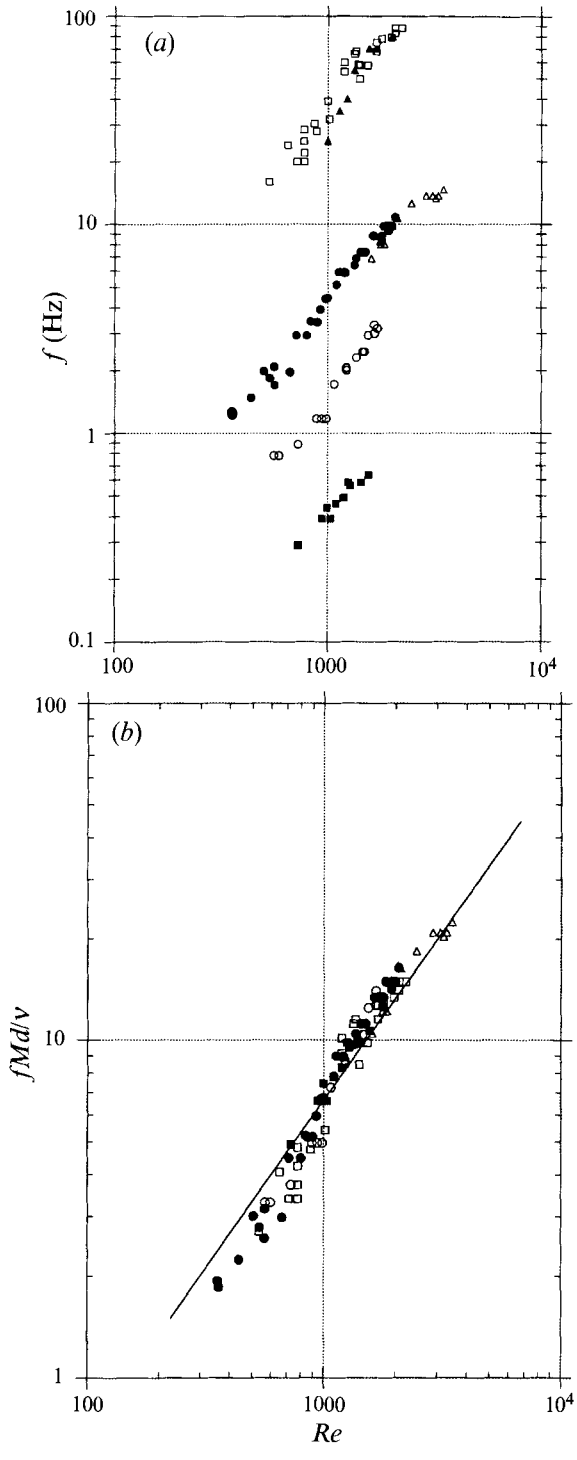

FIGURE 8. (*a*) Merging-distance oscillation frequencies obtained for various grids as a function of the jet Reynolds number. (*b*) Collapse of the measured frequencies, rescalled by fMd/ν, as a function of Re; the solid curve corresponds to $fMd/\nu = 0.007Re$. Square network, $M/d = 2.54$, frequencies determined from velocity fluctuations: □, $d = 1$ mm; ●, $d = 3$ mm; ○, $d = 5$ mm; ■, $d = 10$ mm; from pressure fluctuations: △, $d = 3$ mm. Triangular network, frequencies determined by velocity fluctuations: ▲, $d = 0.8$ mm; $M = 2.73$ mm.

High pulsations ω lead to a small penetration depth ζ, that is to an oscillating plug flow, while low frequencies lead to raccorded boundary layers from $y = \pm\frac{1}{2}M$ to the centre of the cavity, and to a developed viscous oscillating velocity profile.

Let $\langle \delta v \rangle$ be the average of $\delta v(y)$ over the width of the cavity:

$$\langle \delta v \rangle = \frac{\mathrm{i}a}{\omega} \mathrm{e}^{-\mathrm{i}\omega t} \left[1 - \frac{\tan(\frac{1}{2}kM)}{\frac{1}{2}kM} \right]. \tag{12}$$

In accordance with what is stated above, $M/\zeta \ll 2$ leads to a viscous fluctuating flow which oscillates in phase with the driving pressure $a\mathrm{e}^{-\mathrm{i}\omega t}$:

$$\langle \delta v \rangle \approx \frac{aM^2}{12\nu} \mathrm{e}^{-\mathrm{i}\omega t}, \quad M/\zeta \ll 1, \tag{13}$$

whereas $M/\zeta \gg 1$ reveals a phase-shift of $\frac{1}{2}\pi$ between velocity and pressure. In this regime, $\delta v(y)$ is practically constant in the y-direction over the width of the cavity except in the thin adjacent boundary layers where it varies rapidly. This limit amounts to considering a negligible viscosity for which the problem is amenable to a balance between purely inertial and pressure forces implying, by the derivation with respect to time, the quadrature of phase:

$$\langle \delta v \rangle \approx \frac{a}{\omega} \mathrm{e}^{-\mathrm{i}\omega t + \mathrm{i}\pi/2}, \quad M/\zeta \gg 1. \tag{14}$$

The phase shift between velocity and pressure is shown for arbitrary values of M/ζ in figure 10. In our experiments, M/ζ has a typical value of 15, and thus one expects $\delta v(t)$ and $p(t)$ to be nearly in quadrature of phase. This is precisely what is observed on figure 9(*c*), showing the intercorrelation of $\delta v(t)$ and $p(t)$ measured in the centre of a cavity and which are actually phase shifted, with a phase-lag very close to $\frac{1}{2}\pi$.

This simple experiment is helpful in the understanding of the hydrodymamic regime controlling the cavity flow in that it exhibits the dynamical role of the pressure, responsible for the periodic injection of downstream turbulent packets in the recirculating flow (figure 5). We pursue this interpretation in the next section.

3.3. *Large-scale coherence*

The spatial organization of the oscillations has been investigated by using two probes, keeping one fixed at the edge of a jet, and moving the other one along the y-axis at the same x-location (the precise location is, in fact, of little importance since the velocity fluctuations are coherent inside the cavity; in other words, the wavelength associated with the oscillation is much larger than the cavity length). The probes are separated by a variable distance l. The intercorrelation between the two (mean subtracted) signals $\delta v(y, t)$ and $\delta v(y+l, t)$ is calculated according to

$$I(l, \theta) = \lim_{T \to \infty} \frac{1}{T} \int_{-\frac{1}{2}T}^{+\frac{1}{2}T} \delta v(y, t)\, \delta v(y+l, t-\theta)\, \mathrm{d}t. \tag{15}$$

Correlation functions for increasing separation l between the probes are presented in figure 11. As expected for a periodic signal, each correlation function is oscillating with

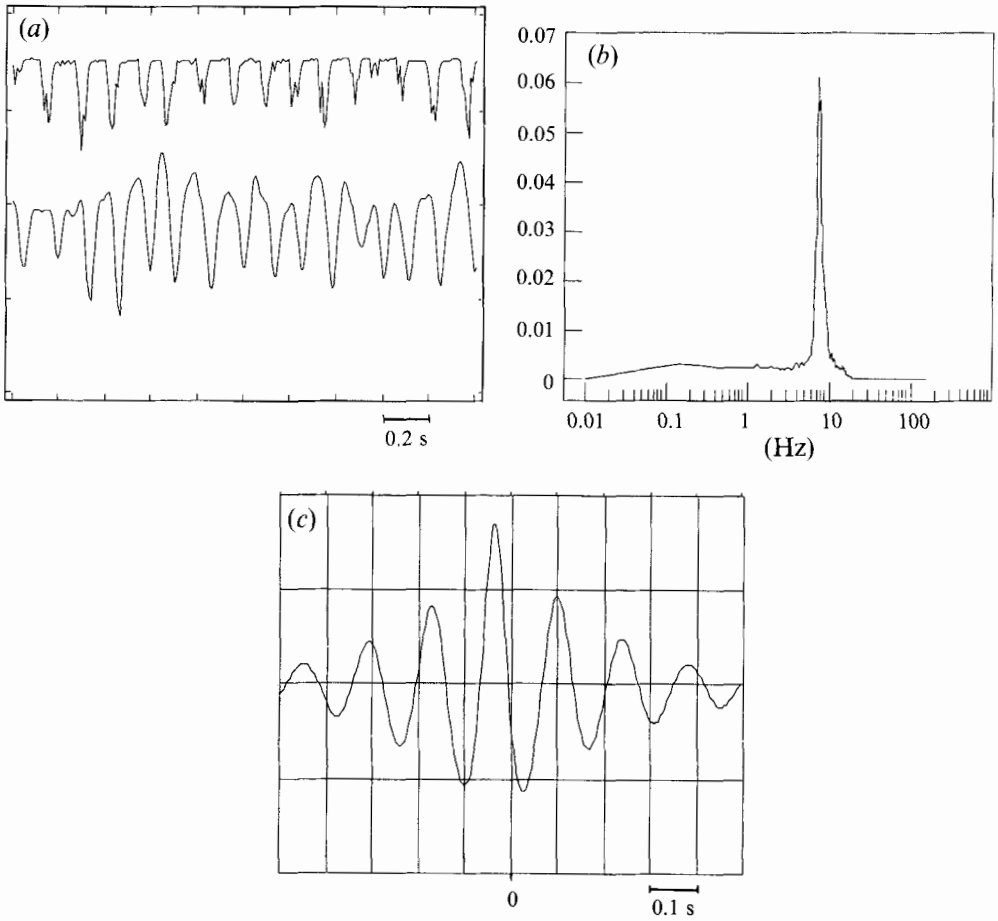

FIGURE 9. (*a*) Simultaneous recordings of the velocity (top) and pressure (bottom) fluctuations at the same location in the centre of a cavity at $x = \frac{3}{4}L$. (*b*) Corresponding power spectrum of the pressure fluctuations. (*c*) Intercorrelation of the velocity and the pressure computed from equation (15) showing a time shift between zero and the time of maximum of correlation very close to a quarter-period (phase lag of $\frac{1}{2}\pi$). Square network, $d = 3$ mm, $Re = 1841$.

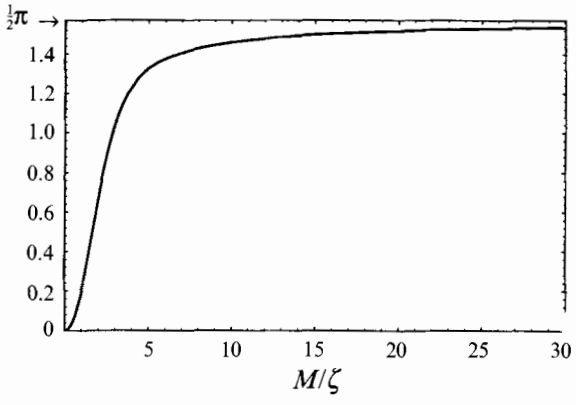

FIGURE 10. Phase shift between velocity and pressure fluctuations in a cavity predicted by equation (12) as a function of M/ζ. In the range of Re covered by our experiments, a typical value for M/ζ is 15.

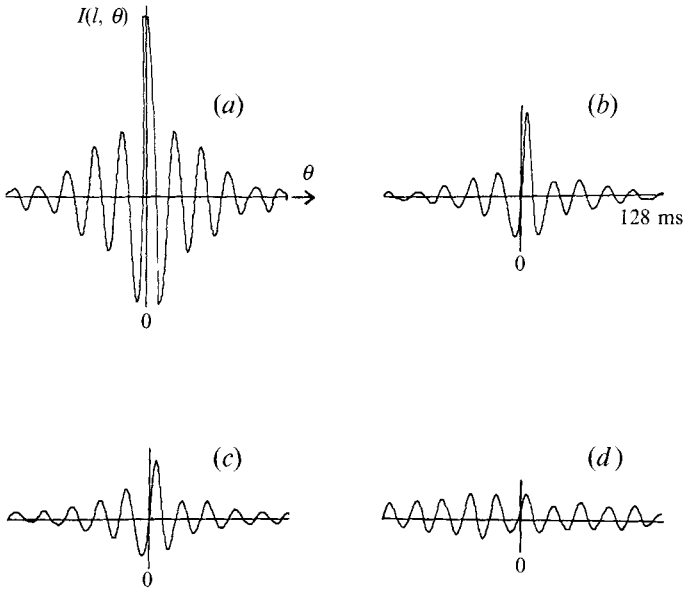

FIGURE 11. Intercorrelation functions for increasing probe separation l. (*a*) $l/M = 0$, (*b*) $l/M = 6$, (*c*) $l/M = 12$, (*d*) $l/M = 20$. Square network, $d = 1$ mm, $Re = 2574$.

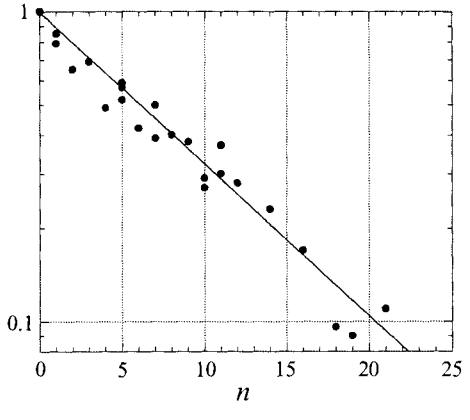

FIGURE 12. Maximum correlation as a function of distance l expressed in terms of number of jets ($n = l/M$) in the y-direction. The spatial correlations decay exponentially. Square network, $d = 3$ mm, $Re = 1289$.

time separation θ. The damping of the autocorrelation function with respect to θ indicates that the oscillation is fairly noisy. This damping is stronger at the first half-oscillation, which is due to the presence of small-scale turbulence in the regions of lower velocity when the probe is downstream of the merging length. The maximum of the intercorrelation is also damped with increasing separation l. The evolution of the maximum of the correlation as a function of l (or of the number of neighbour from the reference jet) is well representated by an exponential decrease (figure 12) indicating that the coherence of the oscillations remains localized within a circular region 10 to 15 mesh sizes wide. This correlation length is homogeneous over the network and does not depend significantly on the direction y or z nor on the Reynolds number of the jets.

A main feature of these intercorrelations is that they are not symmetric, or parity

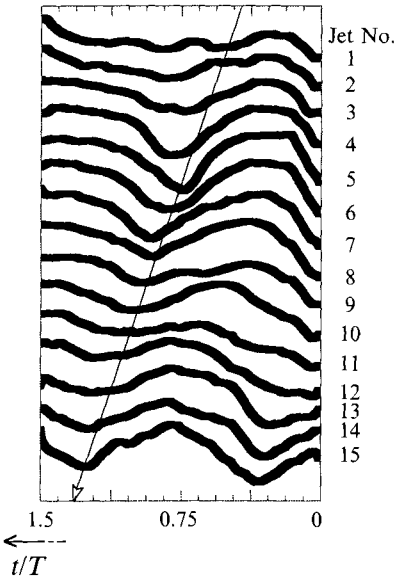

FIGURE 13. Simultaneous evolutions of the amplitude of 15 neighbouring jets, superimposed one over the other in arbitrary units (cut of the network in the y-direction), over one and a half periods. The arrow indicates the direction of wave propagation, which is directed towards the centre of the network.

invariant. Standing waves would produce symmetric intercorrelation curves. The maximum of intercorrelation is time shifted, and the shift increases with probe separation l. This feature is the signature of a propagation mechanism in the plane of the grid. As we were investigating the existence of propagation of the waves in the y- and z-directions, we found that it was systematically detected when the mean position of the two probes was not precisely at the centre of the network. The direction of the wave propagation was also systematically found to be directed from the boundaries of the network to the centre.

The visualizations reflect this property as well. Since the period of oscillation is large compared with the sampling period of the camera, it is possible to follow the space–time evolution of the amplitude of an array of jets seeded with smoke. One clearly sees on figure 13, showing 15 adjacent jets labelled from 1 to 15 beginning at the upper boundary of the network in the y-direction, the spatial phase shift of a wave one-and-a-half periods long, oriented towards the centre of the network.

A physical description that aims to be compatible with all of the above-reported observations has to be able to explain the origin of the oscillatory behaviour, as well as the spontaneous symmetry breaking of the phase along the network. We present now a possible model which has as essential ingredient the existence of a recirculating flow in the cavity adjacent to each jet. The extension of this model to other unstable recirculating flows will also be outlined.

4. The nonlinear delayed saturation (NLDS) model

4.1. *Origin of the oscillations: delayed saturation*

The fact that fluids flowing near obstacles or through confining devices may develop and maintain self-sustained oscillations of velocity and internal pressure has been known for a long time. Rockwell & Naudascher (1979) review the basic configurations

of shear layer and impingement edge geometries that produce self-sustained oscillations. The mechanism of the oscillations is usually claimed to be related to the coupling between the vortex impingement or separation and the corresponding associated pressure field. A generic example of these situations is a convective flow, like a jet for instance, liable to develop shear instabilities and which impinges at a given distance from the nozzle on an edge or on a plate (the 'edge tone', Powell 1961; Crighton 1992). A pressure wave originating in the impingement of a vortical structure on the obstacle travels upstream and may thus trigger the shedding of a new vortical disturbance at the nozzle, provided that the convective timescale of the vortices and the pressure feedback travel time satisfy a certain resonance criterion (Ho & Nosseir 1981). In the terminology of Chomaz, Huerre & Redekopp (1988) (see also Huerre & Monkewitz 1990), the flow is still convectively unstable, but dominated by a pressure loop in contrast to flows that are intrinsically absolutely unstable, that is to say flows in which vorticity disturbances grow locally faster than they are convected downstream. These unstable flows may present, in a certain region of space, a hydrodynamic resonance which has been, for example, observed for jets issuing into an environment of different density (Monkewitz *et al.* 1990).

Among the different configurations quoted by Rockwell & Naudascher, flows developing spatially in the vicinity of and interacting with rigid cavities are also mentioned as giving rise to oscillating separation and reattachment. This is particularly the case for the flow over a backward-facing step which is known, when the Reynolds number based on the step height is not too small, to present an unsteady quasi-periodic reattachment process at the floor downstream of the step (Eaton & Johnston 1980, 1982; Berman 1965). Since this pattern is directly related to the case of multiple jets, for which the recirculation is the dominant feature of the cavities, we will focus on the understanding of the dynamics of this class of flows, where the feedback loop is realized physically by a *recirculation of mass*, whose hydrodynamical state is, as for neighbouring jets above a critical Reynolds number, more or less turbulent.

The starting point of our interpretation is the model of Landau for weakly nonlinear instabilities (Landau 1944; Landau & Lifchitz 1989) which we briefly summarize here. To prevent the unphysical exponential growth of an instability amplitude $A(t)$ at long times, an expansion in $A(t)$ of the variation $\mathrm{d}A(t)/\mathrm{d}t$ up to the first non-zero nonlinear term is considered in the form

$$\frac{\mathrm{d}}{\mathrm{d}t}A(t) = rA(t) - \mu|A(t)|^2 A(t). \tag{16}$$

This very well known model, originally conjectured by Landau in 1944, has found a broad application in hydrodynamics and beyond (Stewartson & Stuart 1971; Fauve 1991) and predicts a saturation of the amplitude at large times

$$A(t \to \infty) = (r/\mu)^{\frac{1}{2}}. \tag{17}$$

We take into account this property for the case of recirculating flows and for confined jets in particular by noting that

(i) a free jet does not display remarkable low-frequency oscillations;

(ii) the oscillations come from the confinement, realized either by solid walls or by neighbouring jets;

(iii) the role of the confinement is to establish a recirculating zone adjacent to the jet in the near field which convects large-amplitude perturbations upstream;

and we proceed, heuristically, as follows.

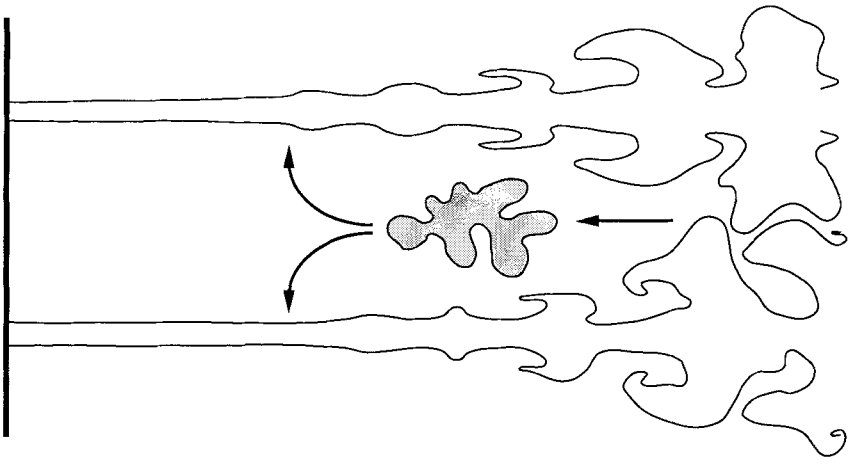

FIGURE 14. Sketch of the recirculation and jet destabilization mechanism. A turbulent packet of fluid, shed at the merging distance of the jets is convected upstream in the cavity. The action of this packet on the initiation of shear instability of the jets is delayed by a time τ, necessary for the packet to escape the merging zone and to travel towards the beginning of the shear instability at the edge of the jets.

We call the recirculation time of the fluid in the cavity τ. This is also the transit time of a 'turbulent blob' shed by the jet at the merging zone and convected upstream, via the recirculation, into the region of the jet where the shear instability is initiated.

In order to model the dynamics of the confined jet, we propose to make the nonlinear saturation effective with a time lag, a delay equal to the time that is necessary for a turbulent packet to be convected upstream from the merging zone towards the beginning of the jet. We thus propose to write the equation describing the time evolution of the relative amplitude ($A(t) \sim \text{constant} - \delta L(t)/L$) of the merging or reattachment length in the form

$$\frac{\mathrm{d}}{\mathrm{d}t}A(t) = rA(t) - \mu\left(\int_0^\infty |A(t-t')|^2 f(t')\,\mathrm{d}t'\right)A(t). \tag{18}$$

In this convolution expression, $f(t)$ is a function that modulates the retarded action of the nonlinear term $|A(t-t')|^2$ on the development of the linear instability, whose kernel is represented by the structure $\partial_t A(t) \sim rA(t)$. The form of the function may be guessed on physical grounds. Its maximum must be located at $t = \tau$ since this instant represents the mean position of an active saturation packet convected upstream in the cavity. This packet has necessarily a certain volume and thus, due to its finite size, may be active during a certain time σ spread around the mean time τ. The general form of $f(t)$ can thus be represented by a Gaussian function, which naturally expresses spreading of variance σ and locality around a mean τ:

$$f(t) = \frac{1}{\sigma\pi^{\frac{1}{2}}}\mathrm{e}^{-\frac{(t-\tau)^2}{\sigma^2}}. \tag{19}$$

We see that, within the purely temporal formalism of (18) and (19), the spatial nature of the developing flow is included in the formulation of the instability dynamics via the spatial meaning of τ and σ (figure 14).

In the following, we will only consider the case of an infinitely localized retarded action, representing the nonlinear delayed saturation (NLDS hereafter) of an eddy,

whose scale is small compared with the dimensions of the cavity ($\sigma \ll \tau$). In this particular case, $f(t)$ is the Dirac delta function located at $t = \tau$ and the dynamical equation of the NLDS model is written

$$\frac{\mathrm{d}}{\mathrm{d}t}A(t) = rA(t) - \mu|A(t-\tau)|^2 A(t). \tag{20}$$

The existence of a continuous and bounded range of retarded times as in (19) does not alter the temporal features of (20) (Villermaux & Hopfinger 1994). The NLDS model given by (20) can be considered as the generic formalism of the physical mechanism presented above, involving a coupling between linear instability and nonlinear delayed saturation.

The parameter r represents the usual instability growth rate, μ stands for the sensitivity to the nonlinearity and τ is the recirculation time in the cavity. The integration of (20) can be performed numerically, and it is shown on figure 15 for different values of r and τ that the amplitude $A(t)$ never reaches a stationary limit when $r\tau > \frac{1}{4}\pi$ (this will be derived later), but oscillates monoperiodically around the value $(r/\mu)^{\frac{1}{2}}$ which cancels the time derivative. Moreover, $A(t)$ always remains positive if $A(0)$ is positive.

One can show that a cycle of oscillation can be decomposed into two exponential branches on suitably chosen intervals of the period. This decomposition mimics the exact solution of $A(t)$ by a set of alternating relaxations, one with a positive argument and the other with a negative argument (a kind of relaxation oscillation, see Villermaux & Hopfinger 1994) and gives

$$rT = r\tau(2 + \kappa + 1/\kappa), \tag{21a}$$

with

$$\kappa = \frac{1-\beta^2}{[(1-\beta)\,\mathrm{e}^{r\tau(1-\beta^2)}]^2 - 1} \quad \text{where} \quad \beta \approx \tfrac{1}{2}. \tag{21b}$$

The parameter β represents, in the expression of the argument of each exponential branch, the maximum and the minimum value of the amplitude with respect to $(r/\mu)^{\frac{1}{2}}$ and, by construction, must be close to $\frac{1}{2}$. The period T is a function of r and τ only whereas μ sets the amplitude of the oscillation. The different physical parameters involved in these expressions can be evaluated in the case of a confined jet as follows. Beyond a critical Reynolds number, the initial growth rate r of the shear layers of a jet is of the order of u/d; this is the growth rate of the shear layer as soon as its width has reached the size of the diameter d, and can also be written $r \sim (\nu/d^2)[Re - Re_c]$. For a laminar elongated cavity, the lubrication approximation (equation (3)) suggests that the maximum recirculation velocity, obtained at the centre of the cavity ($y = 0$) is about $\frac{1}{3}u$. The recirculation time τ is of the order of M/u, which is the time for a turbulent packet to escape the merging zone and to be convected upstream in the cavity by a distance of the order of its own size. It then appears that the product $r\tau$ is independent of the Reynolds number and, accordingly, the frequency of oscillation f is expected to vary linearly with the jet Reynolds number:

$$f = \frac{1}{T} \sim \frac{u}{3M}[2 + (1-\beta)^2\,\mathrm{e}^{2M/d}]^{-1}. \tag{22}$$

The appropriate scaling relation is thus expected to be $fM/u = g(M/d)$ or, alternatively, $fMd/\nu \sim Re$. The function $g(M/d)$ is a function of the geometry of the network only and goes to zero, as expected, when $M/d \to \infty$. It is found from (22) that $g(2.54) = 0.0079$. This value, considering the approximate estimations made for r and

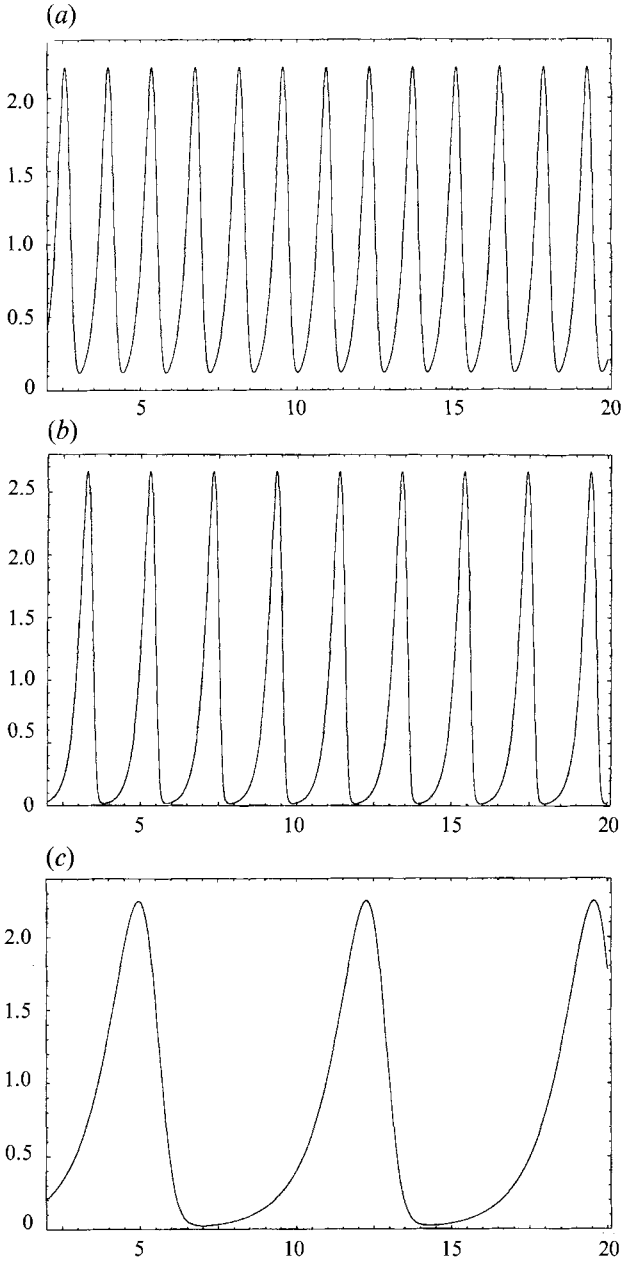

FIGURE 15. Numerical integration of the NLDS model (equation (20)). (*a*) $r = 4$, $\tau = 0.3$, $\mu = 3$; (*b*) $r = 4$, $\tau = 0.35$, $\mu = 3$; (*c*) $r = 1$, $\tau = 1.3$, $\mu = 1$. The amplitude $A(t) \sim \text{constant} - \delta L(t)/L$ remains always positive and displays periodic spikes (see figures 7*a* and 9*a* for comparison).

τ (which are included in the model in their dimensional form and by their orders of magnitude only), compares surprisingly well with the measured one which is close to 0.007 (figure 8*b*). This heuristic model thus displays a good collapse of the jet's oscillations frequencies when rescaled in the proper non-dimensional group and even provides a good estimation for the prefactor $g(M/d)$. It seems that the spatial coupling of the oscillators does not alter substantially the value of the frequency given on purely

geometrical grounds. The amplitude of oscillation is large at low Reynolds numbers, near the onset of the oscillations, and decreases like L with increasing Re (§3 and figure 3). For large Reynolds numbers, the jet is already turbulent near the nozzle, and is no longer excitable by the backflow. In this limit, the self-sustained oscillation vanishes in the turbulent fluctuations of the jet. This effect is taken into account in this model recalling that $\langle|\delta L|\rangle/L \sim \langle A\rangle \sim (r/\mu)^{\frac{1}{2}}$, with $r \sim Re$.

4.2. *Spatial coherence of pressure and diffusion of mass*

We now turn to the question of the spatial coupling between the oscillators. In the plane located at a distance $x = L$ downstream and parallel to the plate, the pressure is oscillating in time, at each point of the plane, at the frequency obtained in §4.1. At a given instant, a point A of that plane (figure 2) located, say, downstream of the merging position (whose position is $L-\delta L$ at that time) has a pressure P_A while its neighbour B located at a distance ξ from A before the merging distance (whose position is $L+\delta L$ at that time in point B), has a pressure P_B such that

$$P_A - P_B = \Delta P. \tag{23}$$

This pressure difference (figure 4*b*) is equal to the total pressure increase given by equation (6). Indeed, as shown on figure 4(*b*), this pressure increase occurs over a short interval Δx. The pressure gradient $\partial P/\partial r$ in the plane parallel to the plate evaluated with respect to the spatial coordinate $r = (y^2+z^2)^{\frac{1}{2}}$ is thus of the order of $\Delta P/\xi$, where ξ is the correlation distance for the pressure in that plane.

The equation of motion for an element of fluid shed by a jet in the vicinity of the plane and accelerated with a radial velocity u_r in the pressure field is

$$\frac{\partial u_r}{\partial t} = -\frac{1}{\rho}\frac{\partial P}{\partial r}. \tag{24}$$

The jet 'explodes' at the merging distance quasi-isotropically and thus u_r scales as u; moreover, the acceleration time of the fluid particle is of the order of T which is the correlation time of the pressure pattern in the plane. With these velocity, time and length scales, u, T and ξ, the equation of motion is written

$$\frac{u}{T} \sim \frac{\Delta P}{\rho \xi}. \tag{25}$$

With $T = M/(0.007u)$ given by the experiments and equation (22), and with $M/d = 2.54$, giving $S_1/S_2 - (S_1/S_2) = 0.106$, one finds, according to this crude description, that the correlation length is $\xi/M = \frac{0.106}{0.007} \approx 15$. The extent of the pressure correlation is the binding mechanism responsible for the synchronization of the local exciting eddies in each cavity and our measurements indeed show that the oscillators are coupled up to the 10th or 15th neighbour, a correlation distance that is independent of Re (figure 12).

A remarkable consequence of this large-scale synchronization is the redistribution of fluid issuing from one jet in the plane parallel to the network. Figure 16(*a*) is an average of images taken over several periods of oscillation of a jet, imbedded in a square network ($d = 5$ mm, $M/d = 2.54$), seeded with white smoke. A cut of the averaged concentration field on a line parallel to the injection plate at one mesh downstream reveals an exponential decay of the concentration of tracer in the adjacent cavities, extending roughly to the fifth neighbour. The concentration in the first adjacent cavity to the seeded jet is about 60 % of the injection concentration and the concentration in

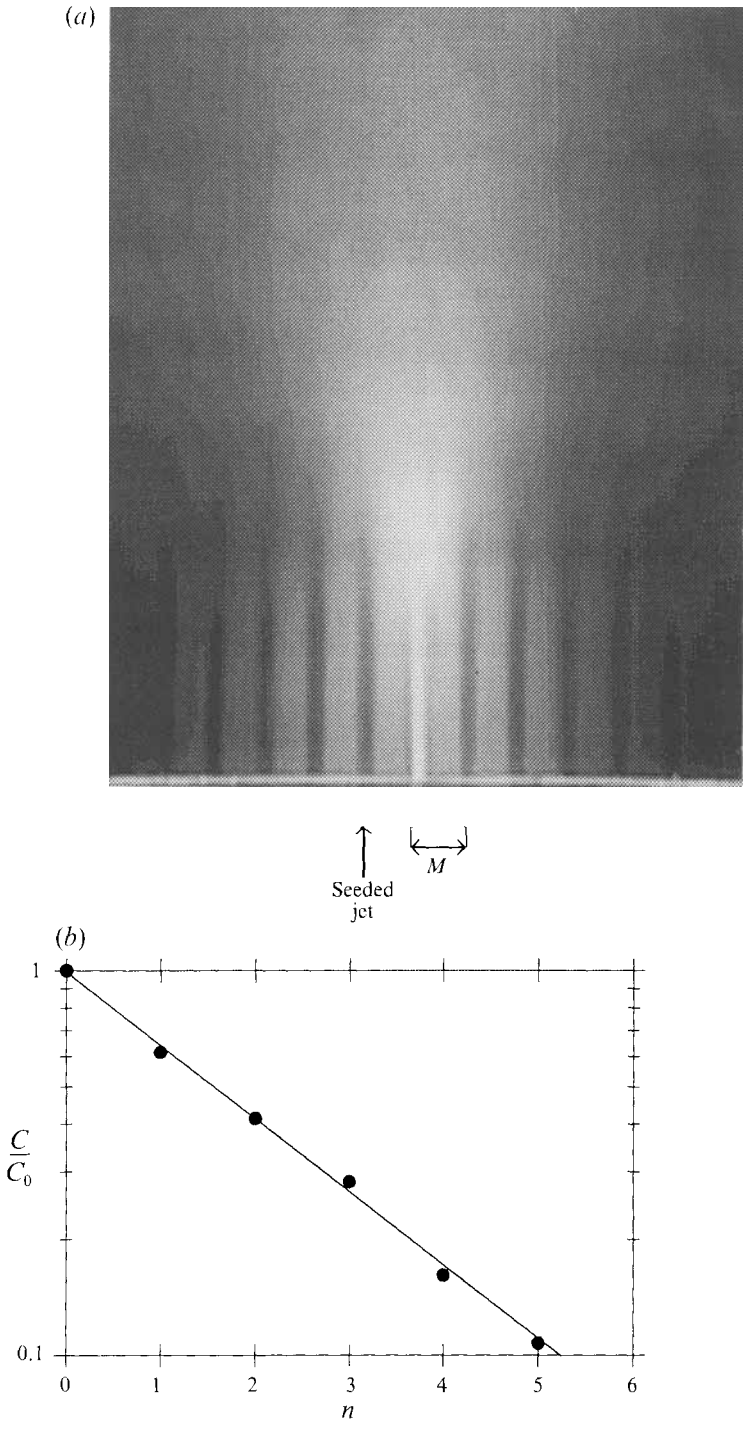

FIGURE 16. (*a*) Mean concentration field around a jet seeded with a white inert smoke. The average has been taken over about 30 periods of oscillation. (*b*) The concentration profile obtained from (*a*) by a cut parallel to the grid at one mesh size downstream from the grid displays an exponential decay on a characteristic scale $\xi_c/M \approx 3$. Square network, $d = 5$ mm, $Re = 1150$.

the fifth cavity is still 10% of the injection value (figure 16*b*). It is important to note that the long-range mass diffusion still occurs at large Re where the amplitude of oscillation has vanished. A simple one-dimensional (but this restriction does not limit the generality of the results) model explains why the diffusion front is non-Gaussian and remains localized in space at infinite times; this is an example of 'anomalous' diffusion (see e.g. Cardoso & Tabeling 1989; Pomeau, Pumir & Young 1989 and Bouchaud & Georges 1990). Let C_n be the concentration of the tracer in cavity n of volume V and width M. We picture the exchanges of mass through the cavity in the following way. The cavity is crossed by an entrainment flow rate q, directed downstream from the core of the cavity to the merging length via the turbulent entrainment by the jets, and the local radial redistribution of mass in the plane parallel to the network at $x \approx L$ (which mainly contributes to the exchange between the cells since the streamlines in the cavities are essentially directed in the x-direction) is accounted for by assuming that the cavity exchanges a flow rate Q with its closest neighbouring cavities labelled $n-1$ and $n+1$. The mass balance of the tracer around the cavity n is then

$$V\frac{\mathrm{d}}{\mathrm{d}t}C_n = -qC_n + QC_{n-1} + QC_{n+1} - 2QC_n. \tag{26}$$

This is a discrete diffusion equation with a loss term (i.e. $-qC_n$) which accounts for the emptying of the cavity by the turbulent entrainment of the adjacent jets. The emptying time $\tau_0 = V/q$ is nevertheless much larger than the transit time τ, and this allowed us to use the 'impermeability' property of the cavity on a period of oscillation in the previous section.

To find the large-scale structure of the concentration profile with respect to the mesh size, we pass to the continuous limit of equation (26), y being again a coordinate parallel to the network:

$$\frac{\partial}{\partial t}C = -\frac{C}{\tau_0} + D\frac{\partial^2}{\partial y^2}C, \tag{27a}$$

with

$$\tau_0 = V/q, \quad D = M^2/R\tau_0 \quad \text{and} \quad R = q/Q. \tag{27b}$$

If, as in the experiment described in figure 16, a point in the y-space ($y = 0$ for instance) is saturated for all times with a tracer of concentration C_0, this model predicts that the concentration front $C(y, t)$ becomes, at large times, stationary and localized on a characteristic lengthscale ξ_c such that

$$C(y, t \to \infty) = C_0 \mathrm{e}^{-y/\xi_c}, \tag{28a}$$

with

$$\xi_c^2 = M^2/R. \tag{28b}$$

The lengthscale ξ_c is related with, but not strictly equal to, ξ the correlation distance for pressure. In spite of the fact that, in the construction of the model, only the exchanges between first neighbours have been taken into account, the typical width of the concentration profile ξ_c may be larger than the mesh size M and this, as expected, is more pronounced when the exchange flux Q is large compared with the emptying flux q (that is to say $R \ll 1$). The refinement of this model to include the exchange for N adjacent neighbours does not raise any difficulty and leads to $\xi_c^2 = \alpha M^2/R$, with $\alpha = \sum_{j=1}^{N} j^2$. Since both q and Q are proportional to each other due to the mass conservation of carrying fluid, their ratio $R = q/Q$ and therefore the width of the diffusion front is expected to be independent of Re for a given geometry. We find, for two-dimensional square networks, $\xi_c/M \approx 3$ (figure 16*b*).

4.3. *Spatio-temporal dynamics*

The central result of the previous section is that the correlations in the cross-plane are, although localized, long-ranged compared with the mesh size. This point is crucial as far as the spatial arrangement of the phase of the oscillation is concerned. The tracer dispersion experiment discussed above reveals moreover that the redistribution of mass is very strong at short distance. Since the fluctuation of the jets is closely linked to the fluctuation of pressure (§3 and figure 9), it is natural to relate the evolution of the amplitude of an oscillator to the amplitude of its closest neighbours by a 'diffusive' coupling. Indeed, this kind of coupling reflects the strong local correlations. The evolution of the amplitude A_n of the oscillator n may thus be written, in one dimension (again, the generalization to the two-dimensional problem is trivial and does not modify the results discussed in the following) in the form

$$\frac{\mathrm{d}}{\mathrm{d}t}A_n(t) = rA_n(t) - \mu|A_n(t-\tau)|^2 A_n(t) + c[A_{n-1}(t) + A_{n+1}(t) - 2A_n(t)]. \tag{29}$$

The parameter c stands for the intensity of the diffusive coupling between the oscillator n and its neighbours $n-1$ and $n+1$ whereas the temporal forcing of the oscillator n keeps the form of the NLDS model.

The linear instability analysis of the dynamical equation can be performed around the fixed point $A_n = (r/\mu)^{\frac{1}{2}}$ by writing, for example, the amplitude $A_n(t)$ as the product of the fundamental temporal solution of equation (20) $A(t)$ modulated by a factor of order unity which incorporates a small real perturbation function of space and time that we write

$$A_n(t) = A(t)f(n,t), \tag{30a}$$

$$f(n,t) = 1 + \varepsilon(n,t), \tag{30b}$$

$$\varepsilon(n,t) = \varepsilon\, \mathrm{e}^{st - \mathrm{i}kMn} + \text{c.c.} \tag{30c}$$

This decomposition is equivalent to the more classical one: $A(t) = A_s(1+\varepsilon(n,t))$ with $A_s = (r/\mu)^{\frac{1}{2}}$. Substitution in (29) gives, to leading order in ε, the dynamical equation for the perturbation:

$$\frac{\mathrm{d}}{\mathrm{d}t}\varepsilon(n,t) = -2r\varepsilon(n,t-\tau) + c[\varepsilon(n+1,t) + \varepsilon(n-1,t) - 2\varepsilon(n,t)]. \tag{31}$$

Taking into account the fact that s is *a priori* complex and decomposing $s = s' + \mathrm{i}s''$, one finds the dispersion relation and the condition of marginal stability:

$$s'' = 2r\sin(s''\tau)\,\mathrm{e}^{-s'\tau}, \tag{32a}$$

$$s' = -2r\cos(s''\tau)\,\mathrm{e}^{-s'\tau} - 2c(1-\cos(kM)). \tag{32b}$$

In the spatial continuous limit ($kM \to 0$), we rewrite this set of equations with the following dimensionless variables: $X = s'\tau$, $Y = s''\tau$, $U = r\tau$ and $K = k(cM^2\tau)^{\frac{1}{2}}$:

$$Y = 2U\mathrm{e}^{-X}\sin(Y), \tag{33a}$$

$$X = -2U\mathrm{e}^{-X}\cos(Y) - K^2. \tag{33b}$$

The threshold of instability occurs for $K = 0$ as soon as $U > \frac{1}{4}\pi$, that is precisely at the onset of the oscillatory regime of a single oscillator. The array of coupled oscillators is thus always unstable at large wavelengths. Figure 17 displays the numerical computation of X and Y for arbitrary values of U and K. Figures 17(*a*) and 17(*b*) show

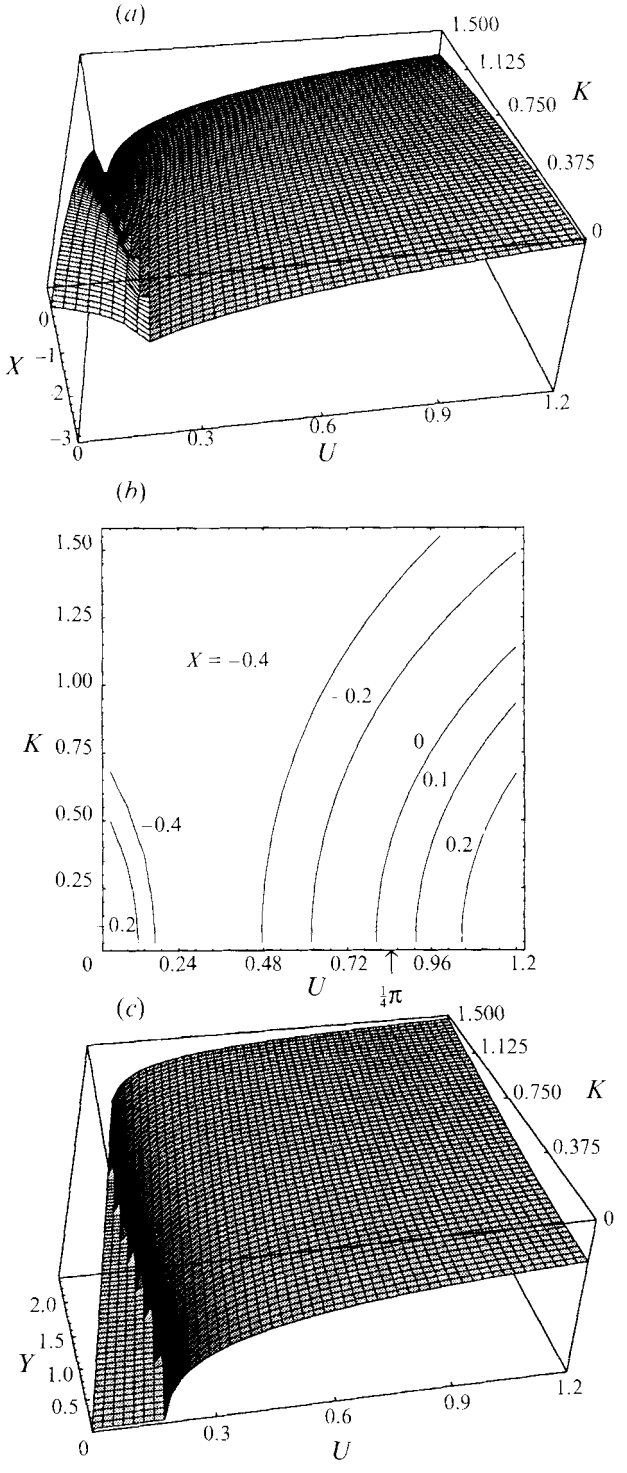

FIGURE 17. (*a*) Linear instability of the model of equation (29). Dimensionless growth rate $X = s'\tau$ as a function of dimensionless wavenumber $K = k(cM^2\tau)^{\frac{1}{2}}$ and delay $U = r\tau$. (*b*) Contour plot of (*a*) for particular values of X. The system is unstable for $k = 0$ as soon as $U > \frac{1}{4}\pi$. (*c*) Same as (*a*) but for the pulsation $Y = s''\tau$.

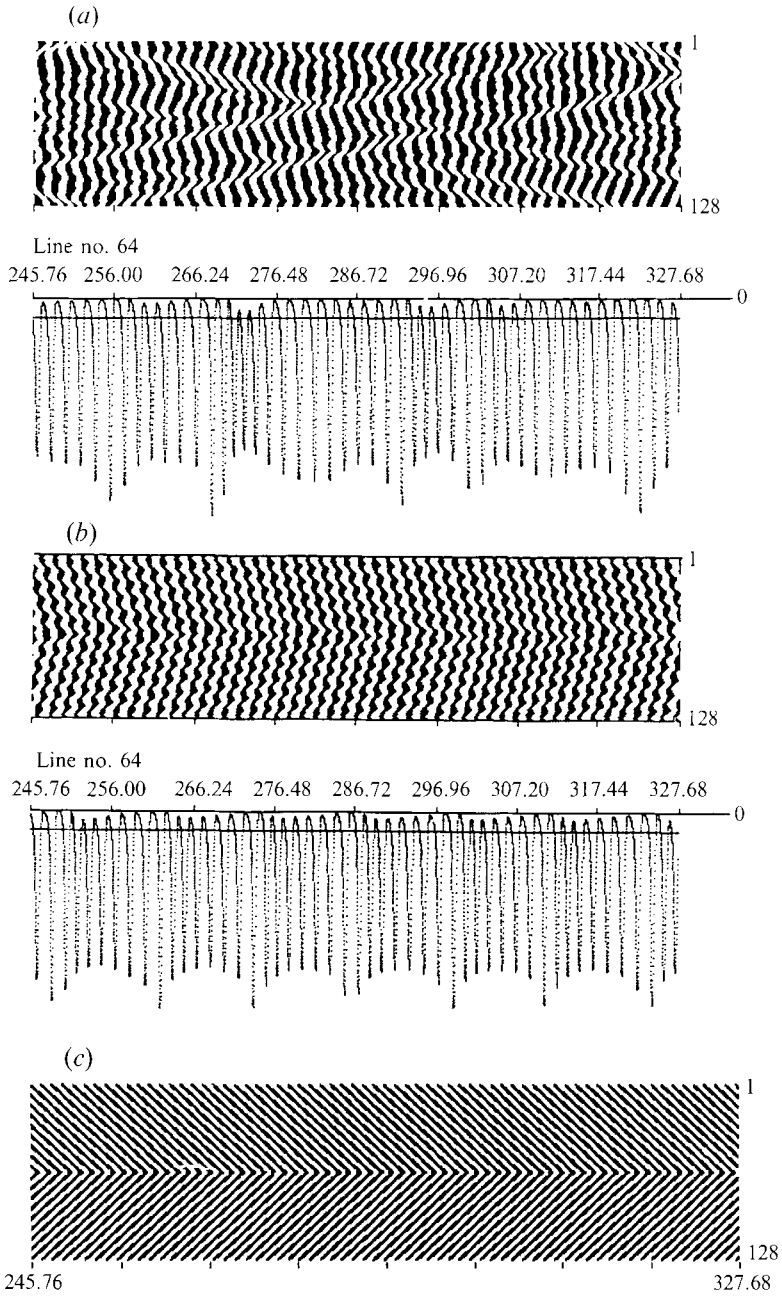

FIGURE 18. Numerical simulation of the model equation (29) with 128 oscillators. Vertical axis = space; horizontal axis = time. In all cases, $r = 4$, $\tau = 0.35$, $\mu - = 3$ and $c = 2$. The dark regions correspond to amplitudes below the threshold shown on the trace of the central oscillator (labelled 64). (*a*) Periodic boundary conditions (oscillator 1 is coupled with oscillator 128). (*b*) Boundary oscillators forced to zero. (*c*) Boundary oscillators forced to $(r/\mu)^{\frac{1}{2}}$.

that the amplification rate X of an unstable mode of wavenumber K is a decreasing function of K. One thus expects the existence of an unstable travelling wave at a scale of the order of the total width of the network. A numerical simulation of this model for an array of 128 oscillators reproduces all of these observations, namely

(i) the existence of a quasi-periodic regime for each oscillator given to a first approximation by (20);

(ii) the continuous emergence of large-scale propagative waves along the network and a strong local coherence;

(iii) the role of the boundary conditions on the directivity of the waves. If the boundary oscillators are forced to zero, a condition which is probably appropriate and representative of finite-size network, the waves are directed from the periphery of the network to the centre.

The third observation is consistent with the existence of the time-shifted intercorrelations discussed in §3 (see also figure 11 and 13). We see from figure 18 that the lines of constant phase in this space–time representation are organized in a chevron-like pattern directed towards the centre of the array and presenting weak secondary instabilities. The group velocity of the waves $v_g = \partial s''/\partial k$, derived from the linear instability for a given selected wavenumber k and its corresponding pulsation s'' and amplification rate s' is given by

$$v_g = \frac{8r\tau cM^2 k \sin(s''\tau)\,\mathrm{e}^{-s'\tau}}{1+(2r\tau\,\mathrm{e}^{-s'\tau})^2-4r\tau\cos(s''\tau)\,\mathrm{e}^{-s'\tau}}. \tag{34}$$

This pattern is reminiscent of the organization of the cellular structures observed in two-dimensional forced convection (Daviaud, Burnol & Ronsin 1991) and, although reversed, of the shape of the vortex tubes shed in the wake of a cylinder at low Reynolds numbers (Williamson 1989; Albarède, Provansal & Boyer 1990; Albarède & Monkewitz 1992). The chevron pattern is even more pronounced when the boundary oscillators are forced to $(r/\mu)^{\frac{1}{2}}$ (figure 18*c*), a value that, like the zero value, cancels the time derivative of the fundamental temporal mode, but contributes more strongly, by diffusive coupling, to the amplification rate of the next neighbours.

5. Conclusions and further remarks

This paper is concerned with the oscillatory instability observed in planar periodic arrangements of jets. The dominant observation is the large-amplitude self-sustained quasi-periodic oscillation of the merging distance of each jet with its near neighbours. The existence domain of this low-frequency instability lies within a jet Reynolds-number range extending from a few hundred, where the onset of the oscillations is observed, to $3\text{–}4\times10^3$ where the amplitude of oscillation vanishes completely. In this Reynolds-number range, the mean merging distance is a decreasing function of Re and goes down to a lower limit fixed by the network mesh size. The oscillation amplitude follows a parallel evolution and, for large Re, becomes indistinguishable from the turbulent velocity fluctuations of the jet.

At the scale of the mesh size, various measurements such as pressure–velocity cross-correlations and passive tracer diffusion have demonstrated the role of the backflow in the oscillations and suggested a scenario for the instability dynamics. It is observed that, as a consequence of the existence of a weak adverse mean pressure gradient due to the expansion of the jets, some packets of turbulent fluid shed by the jets at the merging distance are periodically convected upstream in the cavity. We further remarked that these 'packets' represent hydrodynamical perturbations localized in space and liable to interfere with the upstream development of jet shear instability. No attempt has been made to study in detail the role of the packets in the initiation of the shear instability of the jet because it is of little importance in the present context. The crucial point is that the interaction of the packets and the jet instability is delayed with

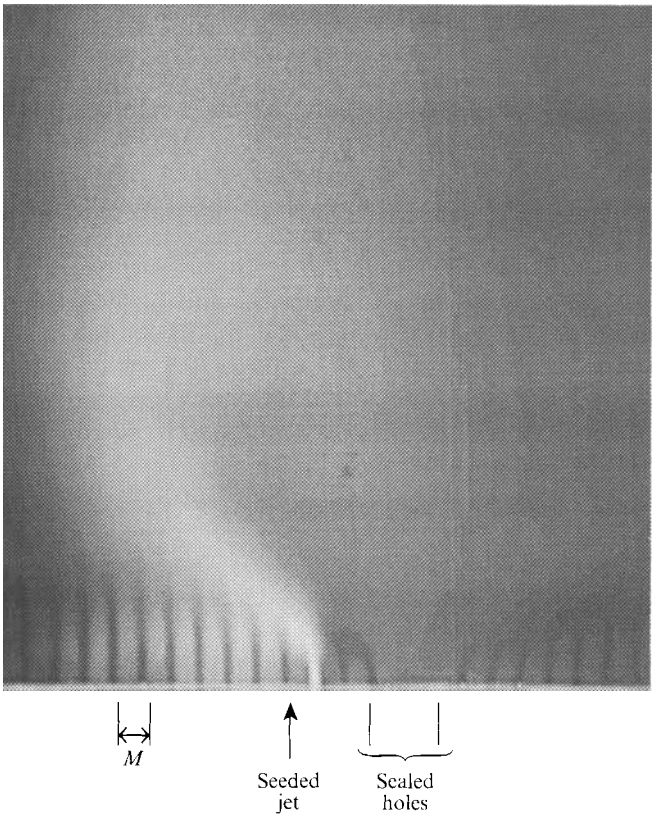

FIGURE 19. Smoke diffusion in a network with defects. In the vertical plane, two holes located two mesh sizes above the seeded jet have been sealed. The consequence of this is the formation of a large recirculation zone downstream of the sealed holes which deflects the nearby jets. Square network $d = 5$ mm, $M/d = 2.54$, $Re = 1885$.

respect to the instant of the packet shedding and that, since it involves a perturbed state far above the critical Reynolds number, it may probably be a nonlinear process. These two ingredients were implemented in a new formalism, called the NLDS model (nonlinear delayed saturation) in the form of an amplitude equation which incorporates a retarded nonlinear term (equation (20) and §4.3). This dynamical equation naturally displays a self-sustained oscillation, the features of which (frequency, amplitude) depend only on the geometry of the confinement of the jets and on Re, in close agreement with the experiments. At the scale of the network, the oscillations, synchronized by the fluctuating pressure gradient, are strongly correlated over a short distance and display the broken-symmetry collective behaviour of large-wavelength travelling waves, directed from the boundaries of the network to its centre (§§3.3 and 4.3).

To close, we would like to suggest two possible future directions for this work.

The first one concerns the spatial arrangement of the jets. In the present study, we considered periodic networks only, square or triangular. It would be interesting, from a practical point of view especially, to consider less ordered networks, including, for instance, defects or modulations of the mesh size. In that case, we expect that the 'holes' in the network, in the sense of the gaps in the network of jet orifices, will dominate the spatial pattern of the near field behind the plate (figure 19). These regions will probably give rise to the formation of large recirculation cavities, possibly

interacting with other neighbouring cavities of the same size, regardless of the presence of smaller-scale cavities in between.

The second one is of a more formal inspiration. One may wonder about the potential generality of the NLDS model. We again draw attention to the fact that this model is a phenomenological formulation and that, therefore, its application may go beyond the problem studied. The flow of a jet confined by solid walls and the flow over a backward-facing step are obvious extensions. In spite of the fact that this model is intended to represent unstable flows with a *convective* recirculation loop, there is no need, strictly speaking at the phenomenological level of the amplitude equation formalism, for this feedbak to be realized by a turbulent convective flow. One could consider if some retro-actions of other physical origin propagating with a finite celerity such as vortical waves (Chomaz *et al.* 1988) or finite-rate chemistry effects in confined combustors (Mitchell, Crocco & Sirignano 1969; Keller 1982) might be accounted for by a formulation of this kind.

Joël Somméria was involved in this work at its early stages and is gratefully acknowledged for his advice, as is Yves Gagne for his interest and experimental suggestions. The authors are deeply indebted to Pierre-Olivier Charpenet for his skills in numerical computation and for his numerous puzzling questions about theoretical formulations. We thank Professor Peter A. Monkewitz for valuable criticisms which helped in clarifying certain points of the paper. This work was financed by the 'Programme de Recherches Coordonnées, Moteurs Fusée' CNRS/CNES/SEP under SEP contract 91-0023C.

REFERENCES

ALBARÈDE, P. & MONKEWITZ, P. A. 1992 A model for the formation of oblique shedding and 'chevron' patterns in cylinder wakes. *Phys. Fluids* A **4**, 744–756.

ALBARÈDE, P., PROVANSAL, M. & BOYER, L. 1990 The Ginzburg–Landau equation as a model for the three-dimensional wake of an elongated bluff body. *C. R. Acad. Sci. Paris* **310** (II), 459–464.

BACK, L. H. & ROSCHKE, E. J. 1972 Shear-layer flow regimes and wave instabilities and reattachment lengths downstream of an abrupt circular expansion. *Trans. ASME* E: *J. Appl. Mech.* 677–681.

BAINES, W. D. & PETERSON, E. G. 1951 An investigation of flows through screens. *Trans. ASME* **73**, 467–480.

BECKER, H. A. & MASSARO, T. A. 1968 Vortex evolution in a round jet. *J. Fluid Mech.* **31**, 435–448.

BERGÉ, P. & DUBOIS, M. 1988 Etude expérimentale des transitions vers le chaos en convection de Rayleigh–Bénard. In *Le Chaos*. Collection CEA, Eyrolles, Paris.

BEARMAN, P. W. 1965 Investigation of the flow behind a two dimensional model with a blunt trailing edge and fitted with splitter plates. *J. Fluid Mech.* **21**, 241–255.

BOUCHAUD, J. P. & GEORGES, A. 1990 Anomalous diffusion in disordered media: statistical mechanisms, models and physical applications. *Phys. Rep.* **4**, **5**, 127–293.

CARDOSO, O. & TABELING, P. 1991 Anomalous diffusion in a linear system of vortices. *Eur. J. Mech.* B/*Fluids* **8**, 459–470.

CHANDRASEKHAR, S. 1961 *Hydrodynamic and Hydromagnetic Stability*. Clarendon Press, Oxford.

CHOMAZ, J. M., HUERRE, P. & REDEKOPP, L. G. 1988 Bifurcation to local and global modes in spatially developing flows. *Phys. Rev. Lett.* **60**, 25–28.

COMTE-BELLOT, G. & CORRSIN, S. 1966 The use of a contraction to improve the isotropy of a grid-generated turbulence. *J. Fluid Mech.* **25**, 657–682.

CORCOS, G. M. 1979 The mixing layer: deterministic models of a turbulent flow. *Rep.* FM-79-2. *Mech. Engng Dept.*, University of California, Berkeley.

CORRSIN, S. 1944 Investigation of the behavior of parallel two-dimensional air jets. *NACA ACR* 4H24.

CRIGHTON, D. G. 1992 The edge-tone feedback cycle; linear theory for the operating stages. *J. Fluid Mech.* **234**, 361–391.

DAVIAUD, F., BURNOL, A. & RONSIN, O. 1991 Travelling and standing waves in a spatially forced 2D convection experiment. *Europhys. Lett.* **16**, 667–672.

DOUADY, S. 1990 Experimental study of the Faraday instability. *J. Fluid Mech.* **221**, 383–409.

EATON, J. K. & JOHNSTON, J. P. 1980 A review of research on subsonic turbulent flow reattachment. *AIAA Paper* 80-1438, pp. 1–11.

EATON, J. K. & JOHNSTON, J. P. 1982 Low frequency unsteadiness of a reattaching turbulent shear layer. In *Turbulent Shear Flows 3* (ed. L. J. S. Bradbury, F. Durst, B. E. Launder *et al.*), pp. 162–170. Springer.

FAUVE, S. 1991 Pattern in Fluid Flow. *Woods Hole Oceanogr. Inst. Tech. Rep. WHOI*-92-16. Woods Hole Oceanographic Institution.

GROTH, J. & JOHANSSON, A. V. 1988 Turbulence reduction by screens. *J. Fluid Mech.* **197**, 139–155.

HO, C. M. & NOSSEIR, N. S. 1981 Dynamics of an impinging jet. Part 1. The feedback phenomenon. *J. Fluid Mech.* **105**, 119–142.

HUERRE, P. & MONKEWITZ, P. A. 1990 Local and global instability in spatially developing flows. *Ann. Rev. Fluid Mech.* **22**, 473–537.

KELLER, J. J. 1982 Nonlinear self-excited acoustic oscillations within fixed boundaries. *J. Fluid Mech.* **123**, 267–281.

LANDAU, L. D. 1944 On the problem of turbulence. *C. R. Acad. Sci. URSS* **44**, 311–314.

LANDAU, L. D. & LIFCHITZ, E. M. 1989 *Mécanique des Fluides.* Moscow: Mir.

MANNEVILLE, P. 1991 *Dissipative Structures and Weak Turbulence.* Academic.

MITCHELL, C. E., CROCCO, L. & SIRIGNANO, W. A. 1969 Nonlinear longitudinal instability in rocket motors with concentrated combustion. *Combust. Sci. Tech.* **1**, 35–64.

MONKEWITZ, P. A. & BECHERT, D. W., BARSIKOW, B. & LEHMANN, B. 1990 Self-excited oscillations and mixing in a heated round jet. *J. Fluid Mech.* **213**, 611–639.

POMEAU, Y., PUMIR, A. & YOUNG, W. 1989 Anomalous diffusion of tracer in convection rolls. *Phys. Fluids* A **1**, 462–469.

POWELL, A. 1961 On the edgetone. *J. Acoust. Soc. Am.* **33**, 395–409.

ROCKWELL, D. & NAUDASCHER, E. 1979 Self-sustained oscillations of impinging free shear layers. *Ann. Rev. Fluid Mech.* **11**, 67–94.

SAARLOOS, W. VAN & HOHENBERG, P. C. 1992 Fronts, pulses, sources and sinks in generalized complex Ginzburg–Landau equations. *Physica* D **56**, 303–367.

SOMMÉRIA, J. 1986 Experimental study of the two dimensional inverse energy cascade in a square box. *J. Fluid Mech.* **170**, 139–168.

STEWARTSON, K. & STUART, J. T. 1971 A non-linear instability theory for a wave system in plane Poiseuille flow. *J. Fluid Mech.* **48**, 529–545.

TABELING, P., CARDOSO, O. & PERRIN, B. 1990 Chaos in a linear array of vortices. *J. Fluid Mech.* **213**, 511–530.

VILLERMAUX, E. & HOPFINGER, E. J. 1994 Self-sustained oscillations of a confined jet: a case study for the non-linear delayed saturation model. *Physica* D (to appear).

VILLERMAUX, E., SOMMÉRIA, J., GAGNE, Y. & HOPFINGER, E. J. 1991 Oscillatory instability and genesis of turbulence behind a high solidity grid. *Eur. J. Mech.* B/*Fluids* **10**, 427–439.

WILLIAMSON, C. H. K. 1989 Oblique and parallel modes of vortex shedding in the wake of a circular cylinder at low Reynolds numbers. *J. Fluid Mech.* **206**, 579–627.

YU, K. H., TROUVÉ, A. & DAILY, J. W. 1991 Low-frequency pressure oscillations in a model ramjet combustor. *J. Fluid Mech.* **232**, 47–72.